NANO LETTERS

2004
Vol. 4, No. 2
197−204

Ultrafast Carrier Dynamics in Single ZnO Nanowire and Nanoribbon Lasers

Justin C. Johnson,[†] Kelly P. Knutsen,[†] Haoquan Yan,[†,‡] Matt Law,[†,‡] Yanfeng Zhang,[†,‡] Peidong Yang,*[,†,‡] and Richard J. Saykally*[,†]

Department of Chemistry, University of California, Berkeley, California 94720 and Materials Science Division, Lawrence Berkeley National Laboratory

Received September 16, 2003; Revised Manuscript Received October 15, 2003

ABSTRACT

Time-resolved second-harmonic generation (TRSHG) and transient photoluminescence (PL) spectroscopy are utilized to probe the ultrafast creation and subsequent relaxation of excited carriers immediately following band-gap excitation in single ZnO nanowire and nanoribbon lasers. The TRSHG signal consists of a 1–5 ps recovery present only during strong lasing and a 10–80 ps intensity-dependent component. The transient PL response from single structures exhibits an 80 ps decay component independent of pump power (free exciton PL), and a < 10 ps power-dependent component (stimulated emission) that shifts to earlier delay by ca. 10 ps at high pump fluence.

Optical probing of ultrafast dynamics in nanostructured materials has yielded many new insights into the quantum-confined and surface-mediated behavior of excited carriers.[1−3] Ultrafast above band-gap excitation in direct II−VI or III−V materials excites a large carrier density (typically $10^{17}-10^{20}$ cm^{-3}) of valence band electrons into conduction band states. These excited carriers have been shown to undergo rapid (<100 fs) thermalization and subsequent radiative or nonradiative decay (<1 ns).[4] Photoluminescence upconversion (PLU) and fast-gated transient photoluminescence (PL) studies have yielded information about the radiative recombination of excited electrons and holes. Transient absorption (TA) measurements have probed both ground-state bleaching and excited-state absorption dynamics, further characterizing the transient carrier behavior. In addition, it has been discovered that perturbation of the electron and hole states by quantum confinement produces unique dynamics that are strongly dependent on the nanoparticle size.[3]

In direct-band-gap II−VI highly crystalline bulk materials, radiative decay can be the dominant relaxation pathway, occurring on time scales of several to hundreds of picoseconds. Such materials have fairly high PL quantum efficiency and are useful in a variety of light-emitting devices. However, transformation of the bulk material into nanostructures can enhance nonradiative surface-mediated trapping and collisional effects. Such effects, including Auger recombination,[5] can also occur on a short time scale, competing with radiative decay.[6] Stimulated emission can also influence the short-time dynamics, often obscuring nonradiative decay mechanisms.[7]

The purpose of the present study is to probe the ultrafast carrier relaxation dynamics in single lasing ZnO nanostructures, with the specific aim of elucidating the nature of the carrier behavior near the spontaneous to stimulated emission transition as well as under gain saturation conditions. It is crucial to study single structures, rather than a polydisperse collection, because the lasing threshold and emission behavior of individual structures depend greatly on size, orientation, geometry, and facet quality. Currently, sufficiently monodisperse samples of ZnO wires or ribbons are not available, and studying single structures averts complications arising due to coupling or collective effects. In addition, size effects could play a large role in both surface trapping and in the stimulated emission behavior via waveguiding, thus it is of interest to systematically probe a variety of sizes of individual structures. It should be noted that quantum size effects, such as have been seen in genuine "carrier-confined" nanoparticles, are not expected to be important here, since the typical width/diameter of the nanostructures studied here is almost 2 orders of magnitude larger than the exciton Bohr radius for ZnO (1.7 nm). Modification of the bulk valence and conduction band states is likely to be minimal in these structures, although interband surface states could be more important than in the bulk because of the relatively large surface-to-volume ratio.

Lasing in single ZnO nanowires and nanoribbons has been recently discovered and characterized.[8−10] The thresholds have been observed to be as low as 100 nJ/cm^2 in high quality wires, although typical ribbons show a threshold that is approximately an order of magnitude higher. Observation of a gain profile red shift, as well as individual mode shifting in single structures, has provided indirect evidence that exciton recombination is the primary lasing mechanism at low pump fluence, while electron−hole plasma (EHP)

* Corresponding authors. E-mail: saykally@uclink.berkeley.edu, p_yang@uclink.berkeley.edu
[†] University of California.
[‡] Lawrence Berkeley National Laboratory.

10.1021/nl034780w CCC: $27.50
Published on Web 11/26/2003

recombination may be responsible for gain at higher pumping. The ultrafast dynamics of these two mechanisms has been studied in disordered thin films,[11−14] and a fast decay (several ps) has been observed that is suggested to correlate with stimulated emission, although many details remain unclear. In addition, gain saturation has been observed with pumping at 10−20 times the lasing threshold,[10] the physical mechanism of which has not been fully explored.

The study of radiative decay in single microstructures has been achieved in the past through the combination of microscopic techniques with time-resolved PL or PLU.[15,16] In these studies, a single structure can be isolated and imaged, and the emission can be collected and analyzed, as long as the PL is sufficiently strong. Transient absorption has the advantage that it is capable of probing ground-state bleaching as well as excited-state absorption; however, it is a more difficult technique to apply to individual nanostructures for several reasons: (1) weak absorption for small structures; (2) high background, since the sample does not fill the entire probe spot; (3) high dispersion in microscope objectives, causing temporal delays with a spectrally broad probe.

A more promising approach to the study of ground-state transient properties in single nanostructures is pump−probe harmonic generation. In most cases, the nonlinear signal is generated only in the nanostructure itself, significantly lowering the background noise from the surroundings. Also, the nonlinear susceptibility (especially second-order) is generally more sensitive to changes in structural or electronic symmetry than linear dielectric properties.[17] In materials that are centrosymmetric, the lowest-order nonlinear susceptibility ($\chi^{(2)}$) is zero within the dipole approximation, and second-harmonic generation (SHG) can be observed only at the surface or in regions where the symmetry is broken. Due to this restriction, the SHG signal from centrosymmetric materials is typically very weak, although it can be resonantly enhanced in some cases. Noncentrosymmetric materials, however, can show a fairly large nonresonant SHG signal, and this has been used previously for examination of subtle changes in structural or electronic properties of various materials. For example, the metal−insulator transitions in colloidal Ag nanoparticles[18] and ultrafast phase transitions in GaAs[19] have been observed by monitoring the bulk SHG response. In addition, previous studies of SHG microscopy have elucidated a variety of effects,[20−22] including changes in carrier dynamics associated with defects and interfaces.

A recent study of SHG in ZnO nanowires has shown that achieving a large signal-to-background ratio with single wires on a sapphire substrate is possible.[23] In addition, the polarization dependence of the SHG response shows that the largest $\chi^{(2)}$ component is $\chi^{(2)}_{zzz}$, where z is the direction along the long axis (c-plane) of the crystalline nanowire. The magnitude of this large component should be an excellent probe for changes in the carrier density of the optically excited nanowire.

The effective value of a component of $\chi^{(2)}$ after relatively weak ultrafast excitation can be considered, using a simplified two-level model, as

$$\chi^{(2)}_{\text{eff}} = (N - N_2)\eta\beta_1 + N_2\eta\beta_2 \qquad (1)$$

in which N is the total electron population density that contributes to β_1, the effective second-order hyperpolarizability tensor element of a lattice bond.[24] N_2 is the excited carrier population density, β_2 is the effective hyperpolarizability of the excited carriers, and η is a local-field correction. If β_1 is assumed to be much larger than β_2, then the creation of an excited state population results in a decreased SHG signal, which should scale roughly as ${N_2}^2$, since the detected signal is proportional to $|\chi^{(2)}_{\text{eff}}|^2$. The term η may also be a function of carrier density due to exciton interaction effects, as has been previously suggested;[25] however, it is difficult to decouple this effect from a change in β. Previous studies on transient SHG using relatively low pump fluence have shown that the $\chi^{(2)}_{\text{eff}}$ for a highly noncentrosymmetric material can be considerably lowered by pumping free carriers from the valence band to the conduction band.[22] These excited carriers then no longer contribute to the intrinsically large $\chi^{(2)}$ of the equilibrated material, probably because of the symmetry-breaking associated with excitation to further delocalized states. As the carriers relax to the "ground-state" configuration, the $\chi^{(2)}$ value recovers. The recovery time is thus a combination of the various relaxation mechanisms in the material, including both radiative and nonradiative channels of decay. In contrast to transient PL, the transient SHG is not necessarily sensitive to the nature of the excited carrier, but rather to the removal of ground state electrons. The transient PL signal originates only from recombination of electrons and holes that result in an emitted photon. Thus, the two different techniques, applied over a similar pumping range in a single nanostructure, could provide complementary information about the excitation and relaxation pathways that contribute to the spontaneous and stimulated emission processes.

Details of the synthesis of ZnO nanowires are described elsewhere.[26,27] Wires were removed from the growth substrate by sonication and dispersed onto either sapphire or silicon substrates by drop-casting a solution of the wires onto the cleaned surface. Scanning electron microscopy (SEM) and transmission electron microscopy (TEM) were used to characterize the structural properties of the wires (Figure 1a,b), showing that they have hexagonal cross sections. Wires used in the lasing studies typically had diameters of 100−250 nm and lengths of 3−10 μm. The ZnO nanoribbons in this work were synthesized using two methodologies, which are described in detail in a forthcoming work.[28] The ribbons have lengths of about 10−60 μm, widths of 0.3−3 μm, and thickness near 50−500 nm (Figure 1c,d). Electron diffraction and cross-sectional SEM characterization show that these nanoribbons are single crystalline, they grow along the $[01\bar{1}0]$ direction, and are enclosed by $\pm(2\bar{1}\bar{1}0)$ and $\pm(0001)$ facets, hence possess pseudo-rectangular cross-sections.

The pulsed near-IR probe beam for time-resolved second-harmonic generation (TRSHG) is derived from an optical parametric amplifier (OPA, TOPAS, Quantronix), which is seeded with regeneratively amplified light at 810 nm, from a home-built Ti:sapphire oscillator (88 MHz) and commercial regen/bowtie amplifier (1 kHz, 2.5 mJ, $\approx$ 100 fs pulse

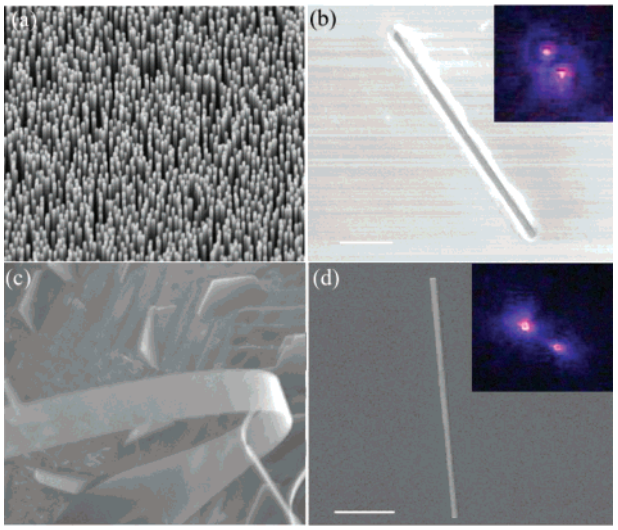

Figure 1. (a) SEM of as-grown nanowire array and (b) single nanowire dispersed on sapphire substrate. Poorly defined edges are the results of charging on the substrate. Scale bar = 1 μm. Inset: far-field image of nanowire emission. (c) SEM of as-grown nanoribbons and (d) single dispersed ribbon on silicon. Scale bar = 5 μm. Inset: far-field image of ribbon lasing emission.

duration, Spectra-Physics, Spitfire). The IR beam is attenuated with a variable neutral density filter to 1−5 μJ per pulse before being focused on the sample with a microscope objective (Olympus, NA = 0.7). The typical spot diameter is estimated to be in the range of 5−20 μm. The intensity in the pump beam is kept low enough so that no PL is generated from multiphoton excitation of the wires, thus perturbing the excited carrier population. The coherent, back-reflected SHG emitted by the nanostructures is collected by the objective, isolated using a dichroic mirror, and focused onto a PMT (Hamamatsu, R3896). The probe wavelength used in most studies is 1400 nm, resulting in SHG at 700 nm. For ultraviolet pumping, 10% of the amplified 810 nm beam is split before the OPA and frequency-tripled, generating a 270 nm beam, which is focused obliquely onto the sample with a fused silica lens. The spot size is kept relatively large (ca. 200 × 100 μm) to achieve uniform illumination of the nanowires or nanoribbons. The PL or lasing emitted from the sample is collected by the microscope objective and is imaged by a video camera at a spatial resolution of 0.5−1 μm. A removable mirror redirects the emission to an optical fiber, which is routed to a spectrograph and CCD (Roper Scientific) for spectral collection with 0.1 nm resolution.

For TRSHG experiments, the pump beam is chopped at a frequency of 500 Hz, and alternating laser shots are collected separately using two gated boxcar integrators. The SHG signal collected with no pump present is subtracted from the signal with pump present, and the result is normalized to the total signal. Approximately 500 shots were averaged at each time step, with signal levels ranging from 10 to 100 photons/shot. The probe is delayed with respect to the pump using a motorized encoded delay stage with step resolution of 5 fs. Transients were collected on both forward and reverse stage scans, and these data were averaged if the scans were reproducible. Cross-correlation measurements of SFG in ZnSe show that the time resolution of the experiment is approximately 200 fs (Figure 2b).

For streak camera experiments, the PL collected from the sample was free-space coupled to the camera (Hamamtsu, C5680) to avoid dispersion effects from the optical fiber. The entire PL/lasing band was collected in each case, and in most cases, multiple pulses were averaged in synchroscan mode to improve the signal-to-noise ratio. Due to triggering jitter in the camera, the temporal resolution was typically limited to about 4 ps (Figure 2c). In single-shot mode, the temporal resolution improved to near 1.5 ps; however, the signal-to-noise ratio was too low for reasonable analysis, except in the cases of the strongest ribbon lasers.

The transient PL response from bulk ZnO (Figure 3a,b) was very similar to what was reported in previous studies.[29,30] The decay fits well to a biexponential function, with a 70−90 ps initial decay (τ_1), followed by a 400−600 ps component (τ_2). The amplitude of τ_2 is typically 60−75% of the total decay, but slowly decreases to near 50% under the highest pumping conditions ($\sim$ 50 μJ/cm^2). Neither decay time has a significant dependence on pump fluence. τ_1 has been attributed to free exciton decay, and τ_2 is thought to be due to bound exciton decay. Both of these decays involve single particle processes, thus their combination produces a two-component exponential decay. The decreased importance of the slow decay with increasing pump fluence is probably due to the saturation of binding sites with increasing carrier density. The saturation of defect PL with increasing carrier density has been previously explored.[10] The amplitude of the free exciton decay continues to increase monotonically with carrier density.

Below the lasing threshold, the single ZnO nanowire transient PL response is quite similar to that of the bulk. τ_1 varies from 75 to 100 ps, while the slow component is difficult to observe. It is possible that the intensity of the slower component may have been below the sensitivity of the streak camera detector. However, once the stimulated emission threshold is reached (as observed in the nanowire emission spectrum), a fast component to the transient PL response is observed, which never appears in the bulk studies. This component has a decay time of approximately 10 ps just above threshold, and it decreases to near 4 ps (the instrument resolution) as the lasing intensity from the nanowire increases. The large disparity between the fast and short lifetimes is attributed to the requirement of population inversion for stimulated emission to occur, which cannot be sustained after the initial cascade of e−h recombination induced by the stimulated emission process. The dynamic range of the detector did not allow for a quantitative measure of the fast decay amplitude versus pumping intensity; however, the amplitude appears to show a highly nonlinear increase just above the nanowire lasing threshold, much like what is observed in the power dependence of the lasing spectrum. In all nanostructures studied, the observation of the fast transient PL component coincided with the appearance of cavity modes in the lasing spectrum. The slower component retains the 75−100 ps lifetime regardless of pump

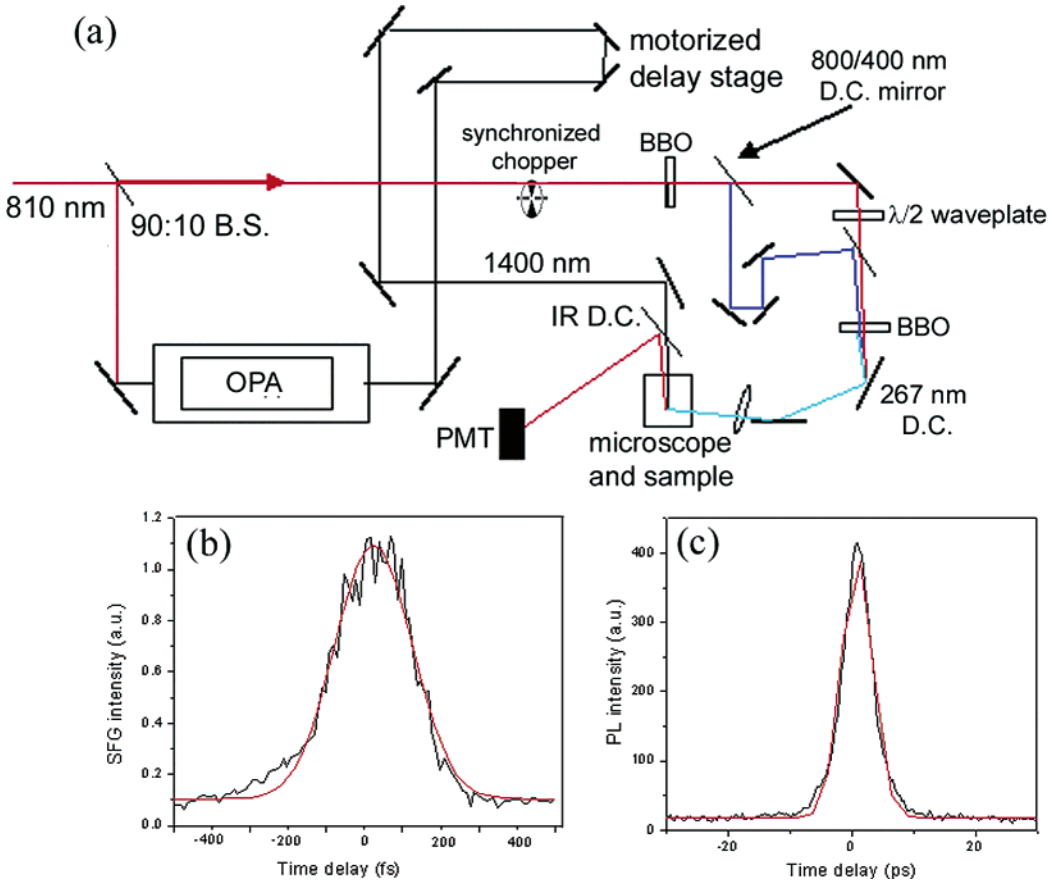

Figure 2. (a) Experimental setup for transient experiments. 810 nm beam is generated by a regeneratively amplified Ti-sapphire oscillator (80 fs pulse width, 1 kHz). The sample is mounted on a 3-axis micrometer stage, with the microscope objective (Olympus, NA 0.7) fixed above the sample, which is monitored with a video camera. A removable mirror directs the PL emission to an optical fiber coupled to a spectrometer and CCD or to the streak camera for transient PL experiments. D.C. = dichroic mirror, B.S. = beamsplitter. (b) Instrument resolution as determined by SFG in ZnSe (fwhm = 200 fs). (c) PL streak camera temporal resolution (fwhm = 4.5 ps).

power. In rigorous terms, if the fast component involves either exciton−exciton or EHP recombination, the decay should follow a $1/N = 1/N_0 + Bt$ dependence, where B is an effective bimolecular rate constant, and N_0 is the excited state population immediately after excitation. However, it was found that the fast decay fit equally well to either model within the signal/noise of the experiment. Contributions from the multiple relaxation pathways may obscure the exact decay form in this case.

In addition to the power dependence of the decay time, the onset of the fast component shifts to earlier time as the pump intensity is increased. In Figure 3d, the short component shifts by ∼10 ps to earlier time from the initial onset of lasing to the highest pumping intensity. The shift occurs rather abruptly (within a 10% change of pump fluence), which strongly suggests that the material undergoes a change in the lasing mechanism from exciton−exciton to EHP recombination. While excitons dominate the dynamics at low pump fluences, increasing carrier density causes a saturation of the exciton population, primarily due to band-filling effects and charge screening. The delay in the onset of the exciton lasing could be due to the relatively long (>5 ps) time necessary for the relatively weak ex−ex interaction to produce sufficient scattering events to allow for the formation of a high concentration of excitons in the appropriate excited state. Electrons and holes in the EHP may quickly thermalize (<100 fs) and form a high density of excited electrons and holes near the band gap, thus creating population inversion and gain. Indirect evidence for this change of lasing mechanism in single wires has been previously obtained in our lab using single-beam, spectroscopic studies;[10] however, the transient results provide a clearer picture of the dynamics associated with the transition. It should be noted that nanoribbon lasers exhibited essentially the same PL decay behavior, although the shift to earlier time of the fast transient typically occurred much nearer the lasing threshold. This is likely due to the higher carrier densities needed to achieve lasing in the ribbons, in some cases leading to EHP dynamics immediately as stimulated emission is reached.

Although the transient PL results elucidate the changes in radiative (i.e., excited state) decay dynamics near the lasing threshold in nanowires, the complete picture of carrier relaxation should include a method of directly probing repopulation of the valence band (i.e., ground state) in order to study nonradiative decay channels. An immediate consequence of the TRSHG sensitivity to $\chi^{(2)}$ is that an instrument-limited (<200 fs) initial SHG loss is observed, correlated with ultrafast (<10 fs) carrier excitation. Unlike in the transient PL results, there is no delay in the onset of SHG loss or recovery, suggesting that the probe is not

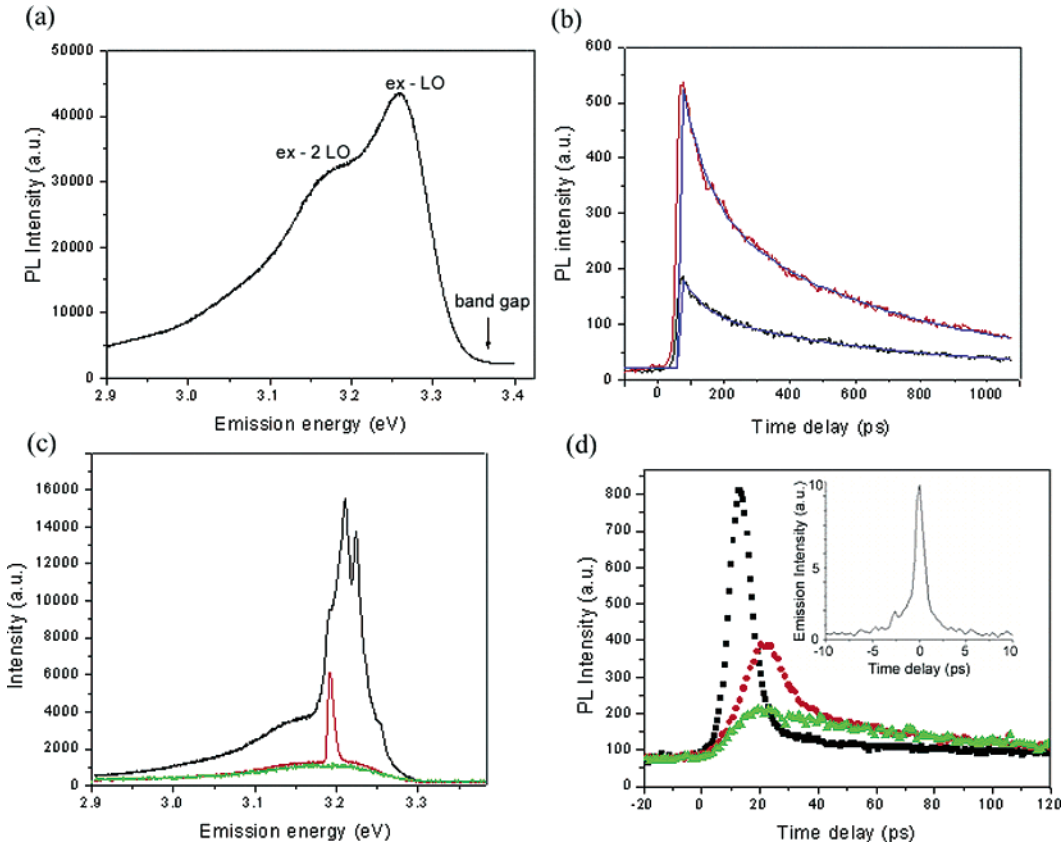

Figure 3. (a) Bulk PL spectrum, showing exciton emission. The broad peaks correspond to phonon-assisted emission. LO phonon energy = 72 meV for ZnO. (b) Transient decay of bulk PL at low (red) ($<5\mu J/cm^2$) and high (black) ($>20\ \mu J/cm^2$) excitation. Fitting to a biexponential decay (blue) gives $\tau_1 = 75 \pm 10$ ps and $\tau_2 = 550 \pm 50$ ps. (c) PL/lasing spectra of single ZnO nanowire near the lasing threshold (excitation $\sim 1\ \mu J/cm^2$) and (d) transient PL response. Long decay component is 70 ± 7 ps and short component is 9 ± 0.8 ps (red) and 4.0 ± 0.3 ps (black). Inset: Single-shot TRPL response from a single nanoribbon.

sensitive to a particular excited species in ZnO, but rather to the loss of valence band electrons. It may be possible using resonance enhancement to probe specifically an exciton resonance, as has been achieved in other experiments;[31] however, this is left for future study. As in the case of e−h recombination, a decay that involves a two-body scattering process (such as ex−ex scattering), should exhibit a $1/\chi^{(2)} \propto t$ dependence. The difference between this dependence and a biexponential including fast and slow components was difficult to discern given the signal-to-noise ratio of the experiment, thus exponential decay times are still reported for comparison purposes.

The transient recovery of the SHG after pumping is practically equivalent in all lasing nanowires and small (width $< 1\ \mu$m) nanoribbons studied. Well below the lasing threshold, the transient SHG response consists of a weak single-component decay (>50 ps). This component becomes more significant near and above the lasing threshold ($> 0.5\ \mu J/cm^2$), and the recovery time shortens to <25 ps (Figure 4d). In the same excitation power range, an additional fast component is observed, the amplitude and decay time of which are plotted as a function of pump fluence in Figures 4c,d. The fast decay time exhibits a decrease from near 5.0 ps just above the lasing threshold to near 1.0 ps near the saturation. The range of decay times and their dependence on excitation fluence for TRSHG is nearly equivalent to the observed PL decay times, suggesting that the relaxation of excited carrier density is strongly influenced by the same process that initiates stimulated emission (inelastic exciton−exciton scattering and annhiliation). However, the SHG transient response appears to be minimally affected by spontaneous emission, and the slower decay of the SHG transient depends much more strongly on excitation power than does the slow transient PL decay. This suggests that a nonradiative decay route also contributes to the slower relaxation, and that this route most likely involves a scattering process, since the recovery time depends on the carrier density. The fast decay component, attributed to stimulated emission relaxation, was not observed in nonlasing structures over a similar excitation range.

Some larger ribbon structures (width $> 5\ \lambda_{PL}$) were also studied using transient SHG, and the behavior of such structures was qualitatively different from the nanowires and small nanoribbons mentioned above. Figure 5b shows transient SHG signal from a single ribbon with width of about 2−3 μm. The PL spectrum (Figure 5a) clearly shows evidence of stimulated emission; however, the transient SHG signal does not exhibit the fast component observed in smaller structures. The decay time is plotted as a function of pump fluence in Figure 5b inset, and again, there is a clear decrease in the decay time with increasing excitation density. These decay times do not match the spontaneous or

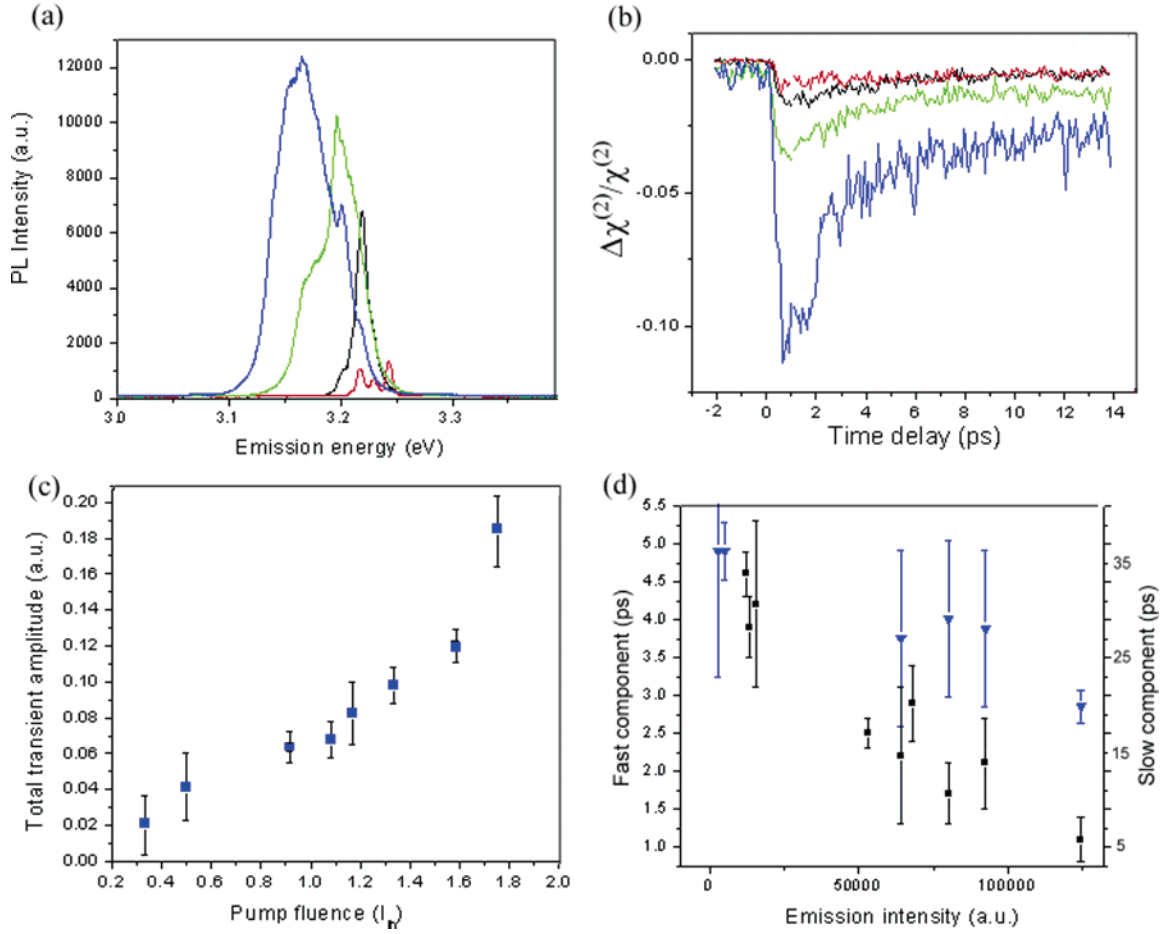

Figure 4. (a) Nanowire laser spectrum and (b) transient SHG response from a single, isolated nanowire. Spectra and transient traces are correlated by color and are taken at pump fluence varying from ~1−5 μJ/cm^2. (c) Plot of the amplitude of the ultrafast $\chi^{(2)}$ loss versus pump fluence in units of the lasing threshold. A nonlinear increase in amplitude is observed as the fast component becomes significant. (d) Fast (black) and slow (blue) component recovery times plotted as a function of the nanolaser emission intensity. The fast component varies nearly linearly with emission intensity, suggesting that stimulated emission and the recovery of $\chi^{(2)}$ are correlated for this feature.

stimulated emission lifetimes discussed earlier, thus it appears that this relaxation is due to a nonradiative decay route involving carrier scattering. The occurrence of stimulated emission without a short decay component is probably due to the size of the ribbon structure. The laser mode volume may be considerably smaller than (or not perfectly aligned with) the volume of material investigated by the IR probe. In this case, the stimulated emission may play only a very minor role in the decay signal, and the nonradiative portion will dominate.

Most nanowires dispersed onto the substrate do not show lasing behavior due to small size, improper orientation, or physical deformities from the sample preparation process. We have studied some of these wires and found that in general there is no fast component of the SHG transient for excitation fluence typically utilized on lasing wires. A very weak slow component (τ = 30−70 ps) is observable, most likely due to a combination of free exciton PL and nonradiative decay. However, upon very high excitation (>25 μJ/cm^2), a subpicosecond decay feature was observed (Figure 6b). The decay time for this fast transient feature is estimated at 400−1000 fs from results on several nonlasing structures. The PL spectrum obtained simultaneously shows a significant increase in multi-phonon-assisted emission as the short time decay appears, indicating a large degree of carrier−phonon coupling. In ZnO, this scattering mechanism (carrier/lattice thermalization) is thought to occur on a subpicosecond time scale due to the strong coupling between charged carriers and the highly polar Zn−O bonds. Evidence for this relaxation mechanism is apparently not observable in the transient SHG response until a very large carrier density is achieved, suggesting that it may proceed via a three-body process. Auger recombination, involving the transfer of electron−hole recombination energy to the kinetic energy of a free electron, is a likely candidate for this decay.[32] The power-dependence of the amplitude and decay time of this transient could not be studied in detail due to limitations on pump power. This decay could also contribute to the short-time TRSHG response in lasing nanowires, but its presence would be obscured by stimulated emission. If these two processes occur on a similar time scale, the nonradiative decay could compete with stimulated emission, causing an effective saturation of the optical gain.[6] The nature of the formation of this early transient is currently under further investigation.

In conclusion, we have demonstrated the first application of TRSHG microscopy for the study of single nanostructures, utilizing the technique to probe both radiative and nonra-

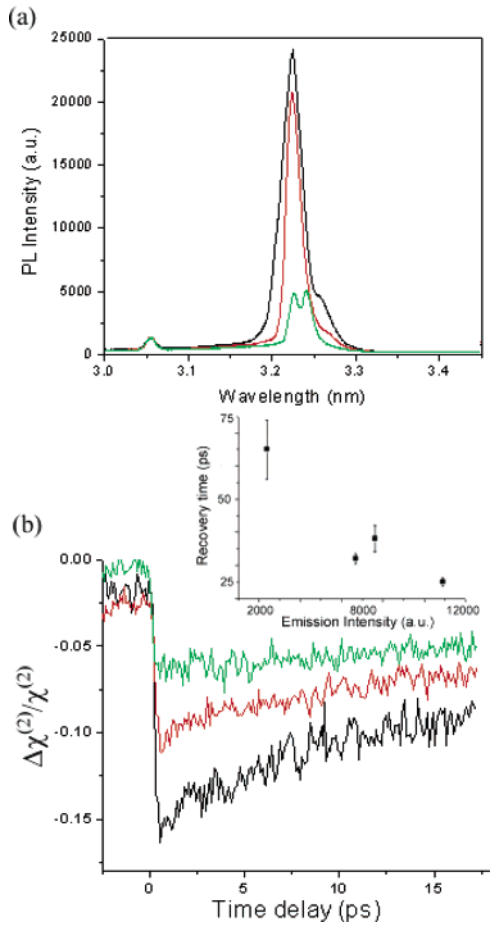

Figure 5. (a) PL spectra from a single ZnO nanoribbon. (b) TRSHG transient signal as a function of excitation pump fluence (excitation ~3−10 μJ/cm^2). Transients are color-coded with spectra. Inset: decay time from monoexponential fit to slow decay time.

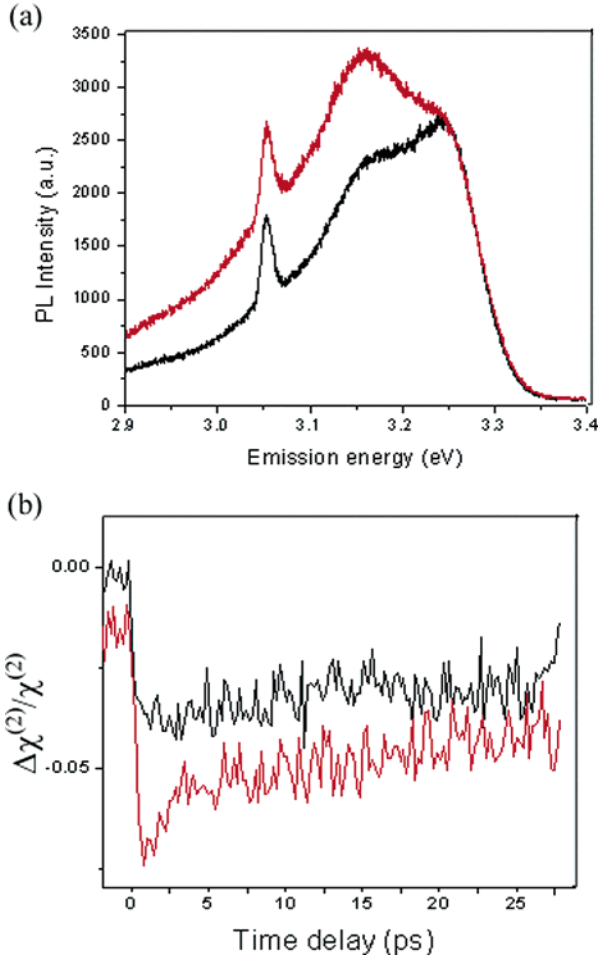

Figure 6. (a) PL spectrum from a nonlasing nanowire and corresponding transient SHG traces (b). Excitation is approximately 20 μJ/cm^2 (black) to near 50 μJ/cm^2 (red). The peak near 3.05 eV is residual laser light from the pump beam.

diative decay processes in highly excited ZnO nanowires and nanoribbons, with several power-dependent recovery times being observed. Transient PL applied to the same nanostructures reveals qualitatively different transient behavior, exhibiting a pump-independent slow component (free exciton decay) also present in bulk ZnO, and a significant fast decay component that is correlated with stimulated emission (exciton−exciton or EHP lasing) only present in nanowires and nanoribbons. The distinct behavior revealed by the two techniques has been attributed to their respective sensitivities to radiative and nonradiative relaxation dynamics. For instance, both techniques produce a slow component (>50 ps) upon low excitation, and high levels of stimulated emission induce a fast component (<5 ps) with an amplitude and decay time that vary strongly with pump power. However, the formation of excitons results in a delay in the transient PL response that is not present in TRSHG, due to the contrasting "ground" and "excited" state sensitivities. In addition, both the slowest and the fastest recovery features in TRSHG exhibit transient behavior characteristic of nonradiative multi-body scattering processes, whereas all transient PL decay components arise from radiative relaxation processes. Exciton−exciton scattering, carrier trapping, and Auger recombination are likely sources of the relaxation observed in TRSHG, although further improvements in sensitivity levels are necessary to allow for quantitative analysis of decay amplitudes and confirmation of the mechanisms of these decay routes. Future studies incorporating resonantly enhanced probing may also provide more detailed information on selected carrier species. In terms of nanostructure geometry, stimulated emission appears to have a smaller effect on the TRSHG response of large nanoribbons, possibly because the waveguide mode volume, unlike that of nanowires, does not fill the probed volume. Other cavity effects such as quality factor and mode confinement, which could affect the emission properties at short times (<300 fs), can be studied with improved transient PL time resolution.

Acknowledgment. R.J.S., K.P.K, and J.C.J are supported by the Physical Chemistry Division of the National Science Foundation. H.Y., M.L., Y.Z., and P.Y. acknowledge the support of the NSF Nanoscale Interdisciplinary Research Team (NIRT) project and the Basic Energy Science, U.S. Department of Energy. We thank Hamamatsu Corporation for use of the streak camera and technical expertise.

References

(1) Klimov, V. I. *J. Phys. Chem. B*, **2000**, *104*, 6122.

(2) Robert, T. W.; Cherepy, N. J.; Zhang; J. Z. *J. Chem. Phys.* **1998**, *108*, 2143.
(3) Mittleman, D. M.; Schoenlein, R. W.; Shiang, J. J.; Colvin, V. L.; Alivisatos, A. P.; Shank, C. V. *Phys. Rev. B* **1994**, *49*, 14435.
(4) Rossi, F.; Kuhn, T. *Rev. Mod. Phys*. **2002**, *74*, 895.
(5) Glinka, Y. D.; Shahbazyan, T. V.; Peraki, I. E.; Talk, N. H.; Liu, X.; Y. Sasaki, Y.; Furdyna, J. K. *Appl. Phys. Lett*. **2002**, *81*, 3717.
(6) Mikhailovsky, A. A.; Malko, A. V.; Hollingsworth, J. A.; Bawendi, M. G.; Klimov, V. I. *Appl. Phys. Lett*. **2002**, *80*, 2380.
(7) Klimov, V. I.; Mikhailovsky, A. A.; Xu, S.; Malko, A.; Hollingsworth, J. A.; Leatherdale, C. A.; Eisler, H. J.; Bawendi, M. G. *Science* **2000**, *290*, 314.
(8) Huang, M.; Mao, S.; Feick, H.; Yan, H.; Wu, Y.; Kind, H.; Weber, E.; Russo, R.; Yang, P. *Science* **2001**, *292*, 1897.
(9) Johnson, J. C.; Yan, H.; Schaller, R. D.; Haber, L. H.; Saykally, R. J.; Yang, P. *J. Phys. Chem. B* **2001**, *105*, 11387.
(10) Johnson, J. C.; Yan, H.; Yang, P.; Saykally, R. J. *J. Phys. Chem. B* **2003**, *107*, 8816.
(11) Zhang, W.; Chai, L.; Xing, Q.; Wang, Q.; Wong, K. S.; Yu, P.; Wange, H.; Tang, Z. K.; Wong; G. K. L. *Chin. Phys. Lett*. **1999**, *16*, 728.
(12) Guo, B.; Ye, Z.; Wong, K. W. *Appl. Phys. Lett*. **2003**, *82*, 2290.
(13) Yamamoto, A.; Kido, T.; Goto, T.; Chen, Y.; Yao, T. *Appl. Phys. Lett.* **1999**, *75*, 469.
(14) Takeda, J.; Jinnouchi, H.; Kurita, S.; Chen, Y. F.; Yao, T. *Phys. Status Solidi B* **2002**, *229*, 877.
(15) Yoshikawa, H.; Sasaki, K.; Masuhara, H. *Chem. Phys. Lett*. **1998**, *293*, 185.
(16) Fujino, T.; Tahara, T. *J. Phys. Chem. B* **2003**, *107*, 5120.
(17) Shen, Y. R. *IEEE J. Sel. Top. Quantum* **2000**, *6*, 1375.
(18) Collier, C. P.; Saykally, R. J.; Shiang, J. J.; Henrichs, S. E.; Heath, J. R. *Science* **1997**, *277*, 1978.
(19) Sokolowski-Tinten, K.; Bialkowski, J.; vonder Linde, D. *Phys. Rev. B* **1995**, *51*, 14186.
(20) Glinka, Y. D.; Shahbazyan, T. V.; Peraki, I. E.; Talk, N. H.; Liu, X.; Sasaki, Y.; Furdyna, J. K. *Appl. Phys. Lett.* **2002**, *81*, 3717.
(21) Bozhevolnyi, S. I.; Maidykovski, A.; Vohnsen, B.; Zwiller, V. *J. Appl. Phys.* **2001**, *90*, 6357.
(22) Schaller, R. D.; Johnson, J. C.; Saykally, R. J. *ChemPhysChem* **2003**, *4*, 1243.
(23) Johnson, J. C.; Yan, H.; Schaller, R. D.; Petersen, P. B.; Yang, P.; Saykally, R. J. *Nano Lett.* **2002**, *2*, 279.
(24) Boyd, R.; *Nonlinear Optics*; Academic: New York, 1992; p. 153. Shen, Y. R. *Principles of Nonlinear Optics*; Wiley: New York, 1984.
(25) Wegener, M.; Chemla, D. S.; Schmitt-Rink, S.; Schafer W. *Phys. Rev. A* **1990**, *42*, 5675.
(26) Huang, M. H.; Wu, Y.; Feick, H.; Weber, E.; Yang, P. *Adv. Mater*. **2001**, *13*, 113.
(27) Yang, P.; Yan, H.; Mao, S.; Russo, R.; Johnson, J.; Saykally, R. J.; Morris, N.; Pham, J.; He, R.; Choi, H.-J. *Adv. Funct. Mater*. **2002**, *12*, 323.
(28) Yan, H.; Johnson, J. C.; Yang, P.; Saykally, R. J. *Adv. Mater*., in press.
(29) Guo, B.; Ye, Z.; Wong, K. S. *J. Cryst. Growth* **2003**, *253*, 252.
(30) Yamamoto, A.; Kido, T.; Goto, T.; Chen, Y. F.; Yao, T. F.; Kasuya, A. *J. Cryst. Growth* **2000**, *214*, 308.
(31) Zhang, W. L.; Wang, H.; Wong, K. S.; Tang, Z. K.; Wong, G. K. L.; Jain R. *Appl. Phys. Lett*. **1999**, *75*, 3321.
(32) Ghanassi, M.; Schanne-Klein, M. C.; Hache, J.; Ekimov, A. I.; Ricard, D. *Appl. Phys. Lett*. **1993**, *62*, 78.

NL034780W